Supporting information

Contents

SI-1 Synthesis Procedures

Synthesis of 9,9-dimethyl-10-[4-(tetramethyl-1,3,2-dioxaborolan-2-yl)phenyl]-9,10-dihydroacridine(B-DMAC) (1)

Potassium acetate(24.3g), 10-(4-bromophenyl)-9,9-dimethyl-9,10-dihydroacridine(7.3g,20mmol) and 4,4,5,5-tetramethyl-2-(tetramethyl-1,3,2-dioxaborolan-2-yl)-1,3,2-dioxaborolane(11.2g,44mmol) were added in a round flask with a stirrer, and the mixture was dissolved in 200ml 1,4-dioxane, then Pd(dppf)Cl_2 (80mg) was added as the catalyst. The mixture was stirred under N_2 atmosphere at 85°C for 36 hours. After the mixture cool to room temperature, 40ml deionized water was added to wash the potassium acetate out, at the same time, used dichloromethane to extract the organic layer. Finally, the column chromatography (dichloromethane: petroleum ether=2:1) was used to gain the product B-DMAC (4.4g, yield=53%).1H NMR (500 MHz, DMSO-d6) δ 8.04 – 7.94 (m, 2H), 7.50 (dd, J = 7.7, 1.6 Hz, 2H), 7.40 – 7.36 (m, 2H), 6.94 (dtd, J = 27.6, 7.2, 1.4 Hz, 4H), 6.14 (dd, J = 8.2, 1.4 Hz, 2H), 1.62 (s, 6H), 1.36 (s, 12H). HRMS(APCI): m/z calcd for $C_{27}H_{30}BNO_2$ $[M+H]^+$ 411.35; found 410.89.

Synthesis of 10-(4-{9-bromonaphtho[2,3-c][1,2,5]thiadiazol-4-yl}phenyl)-9,9-dimethyl-9,10-dihydroacridine (NZ-DMAC) (2)

Potassium carbonate(13.3g), 10-(4-{9-bromonaphtho[2,3-c][1,2,5]thiadiazol-4-yl}phenyl)-9,9-dimethyl-9,10-dihydroacridine(4.4g,10.6mmol) and dibromonaphtho[2,3-c][1,2,5]thiadiazole(3.1g,9mmol) were added in a round flask with a stirrer, and the mixture was dissolved in solution(36ml toluene+24ml THF+24ml

deionized water), then $Pd(PPh_3)_4$(50mg) was added as catalyst. The mixture was stirred under N_2 atmosphere at 90°C for 24 hours. After the mixture cool to room temperature, 30ml deionized water was added to wash the potassium carbonate out, at the same time, used dichloromethane to extract the organic layer. Finally, the column chromatography (dichloromethane: petroleum ether=1:2) was used to obtain the product NZ-DMAC(2.7g, yield=56%).1H NMR (500 MHz, DMSO-d6) δ 8.47 (d, J = 9.0 Hz, 1H), 8.12 (d, J = 9.0 Hz, 1H), 8.00 – 7.92 (m, 2H), 7.85 – 7.75 (m, 1H), 7.72 – 7.60 (m, 3H), 7.55 (dd, J = 7.8, 1.5 Hz, 2H), 7.10 (ddd, J = 8.5, 7.2, 1.5 Hz, 2H), 6.97 (td, J = 7.5, 1.2 Hz, 2H), 6.41 (dd, J = 8.2, 1.2 Hz, 2H), 1.68 (s, 6H). HRMS(APCI): m/z calcd for $C_{31}H_{22}BrN_3S$ $[M+H]^+$ 548.50; found 548.77.

Synthesis of 9,9-dimethyl-10-(4-{9-phenylnaphtho[2,3-c][1,2,5]thiadiazol-4-yl} phenyl)-9,10-dihydroacridine (DMAC-NZP) (3)

Potassium carbonate(4.4g), 10-(4-{9-bromonaphtho[2,3-c][1,2,5]thiadiazol-4-yl}phenyl)-9,9-dimethyl-9,10-dihydroacridine(1.35g,2.5mmol) and boronic acid (3.7g,3mmol) were added in a round flask with a stirrer, and the mixture was dissolved in solution(12ml toluene+8ml THF+8ml deionized water), then $Pd(PPh_3)_4$(15mg) was added as catalyst. The mixture was stirred under N_2 atmosphere at 90°C for 24 hours. After the mixture cool to room temperature, 10ml deionized water was added to wash the potassium carbonate out, at the same time, used dichloromethane to extract the organic layer. Finally, the column chromatography (dichloromethane: petroleum ether=1:3) was used to obtain the product **DMAC-NZP** (764mg, yield=56%).1H NMR (500 MHz, DMSO-d6) δ 8.12 (d, J = 8.9 Hz, 1H), 7.97 (dd, J = 15.3, 8.6 Hz, 3H), 7.72 – 7.50 (m, 8H), 7.12 (t, J = 7.0 Hz, 1H), 6.98 (t, J = 6.9 Hz, 2H), 6.44 (d, J = 8.2 Hz, 1H), 1.69 (s, 6H). 13C NMR (126 MHz, CDCl3) δ 151.51, 151.24, 141.11, 140.95, 136.44, 133.91, 132.01, 131.32, 131.23, 130.80, 130.24, 129.23, 128.54, 128.39, 127.28, 126.80, 126.76, 126.47, 126.43, 125.20, 120.73, 114.34, 36.07, 31.13, 0.01(TMS). HRMS(APCI): m/z calcd for $C_{37}H_{27}N_3S$ $[M+H]^+$ 545.70; found 544.91. Element Analysis for $C_{37}H_{27}N_3S$: C, 81.44; H, 4.99; N, 7.70; S, 5.87; Found: C, 82.24; H, 4.97; N, 7.68; S, 5.489.

Synthesis of 4-{9-[4-(9,9-dimethyl-9,10-dihydroacridin-10-yl) phenyl] naphtho[2,3-c] [1,2,5] thiadiazol-4-yl} benzonitrile (DMAC-NZC) (4)

Potassium carbonate(4.4g), 10-(4-{9-bromonaphtho[2,3-c][1,2,5]thiadiazol-4-yl}phenyl)-9,9-dimethyl-9,10-dihydroacridine (1.35g,2.5mmol) and (4-cyanophenyl)boronic acid (4.4g,3mmol) were added in a round flask with a stirrer, and the mixture was dissolved in solution(12ml toluene+8ml THF+8ml deionized water), then $Pd(PPh_3)_4$(15mg) was added as catalyst. The mixture was stirred under N_2 atmosphere at 90°C for 24 hours. After the mixture cool to room temperature, 10ml deionized water was added to wash the potassium carbonate out, at the same time, used dichloromethane to extract the organic layer. Finally, the column chromatography (dichloromethane: petroleum ether=2:1) was used to obtain the product **DMAC-NZC** (671mg, yield=47%).1H NMR (500 MHz, DMSO-d6) δ 8.15 (dd, J = 8.3, 1.6 Hz, 3H), 8.04 – 7.96 (m, 2H), 7.91 (dd, J = 13.7, 8.5 Hz, 3H), 7.69 – 7.51 (m, 6H), 7.12 (ddd, J = 8.5, 7.2, 1.5 Hz, 2H), 6.98 (td, J = 7.4, 1.2 Hz, 2H), 6.44 (dd, J = 8.2, 1.2 Hz, 2H), 1.69 (s, 6H). 13C NMR (126 MHz, CDCl3) δ 151.19, 150.99, 141.42, 140.93, 136.02, 133.88, 132.32, 132.25, 131.88, 131.84, 131.42, 130.66, 130.30, 128.10, 127.40, 127.21, 126.92, 126.48, 126.27, 125.26, 120.81, 118.79, 114.30, 112.23, 36.08, 31.13, 0.01(TMS). HRMS(APCI): m/z calcd for $C_{38}H_{26}N_4S$ $[M+H]^+$ 570.71; found 569.85. Element Analysis for $C_{38}H_{26}N_4S$: C, 79.97; H, 4.59; N, 9.82; S, 5.62; Found: C, 80.86; H, 4.58; N, 9.84; S, 5.23.

SI-2 Experimental Section

General information (1)

^{1}H NMR and ^{13}C NMR were recorded on a Bruker AVANCZ 500 spectrometer at 500 MHz using deuterated dimethyl sulfoxide (DMSO) as the solvent for ^{1}H NMR and $CDCl_3$ as the solvent for ^{13}C NMR at 298 K. Tetramethylsilane (TMS) was used as internal standards. The MALDI-TOF mass spectra were recorded by an AXIMA-CFRTM plus instrument. The Flash EA 1112, CHNS–O elemental analysis instrument was chosen to characterize these compounds. Single-crystal diffraction measurements

were performed on a Bruker APEXII CCD system. The crystal structures were solved with direct methods and refined with a full-matrix least-squares technique using the SHELXS programs. All angles and distances in crystals were measured using Mercury 2020.3.0 software. The differential scanning calorimetry (DSC, DSC Q100) PerkinElmer thermal analysis system was set at a heating rate of 10 °C min^{-1} and a nitrogen flow rate of 50 mL min^{-1}. Thermal gravimetric analysis (TGA) was performed on a Perkin-Elmer thermal analysis system from room temperature to 800 °C with a heating rate of 10 °C min^{-1}. UV−vis spectra were recorded using a UV-3100 Spectrophotometer. Steady-state fluorescence spectra and fluorescence lifetimes were measured with a FLS980 spectrometer. Corrected PLQY is obtained by manual operation using an integrating sphere apparatus on FLS980. Cyclic voltammetry (CV) was carried out using BAS 100B/W electrochemical analyzer with standard one-compartment, three-electrode electrochemical cell. A glass-carbon disk electrode was selected as a working electrode. Pt wire was performed as a counter electrode. Ag/Ag+ was used as a reference electrode with Ferrocene/ferrocenium (Fc/Fc+) redox couple was used as the internal standard.

Device fabrication and performances (2)

ITO-coated glass was used as the substrate with a sheet resistance of 20 Ω $square^{-1}$. The ITO glass was cleaned by ultrasonic cleaner with deionized water, isopropyl alcohol, acetone and chloroform. The evaporation rate was controlled to be 0.03–0.1 nm s^{-1} for organic layers, 0.01 nm s^{-1} for the LiF layer and 0.3 nm s^{-1} for the Al layer. The PR650 spectra scan spectrometer was used to record EL spectrum and luminance-current density-voltage was measured by spectrometer with a Keithley model 2400 programmable voltage-current source.

Theorical caculations (3)

Density functional theory (DFT) and time-dependent DFT (TD-DFT) calculations were used to describe the ground-state and excited-state properties. For all of the calculations in single molecule, optimized ground- and excited-state geometries were obtained at the levels of M06-2X/6-31G(d,p). For all of the dimers, optimized excited-state

geometries were obtained by using the M06-2X hybrid functional at 6-31G(d,p) level. The natural transition orbitals (NTOs) were evaluated with the dominant "particle"−"hole" pair contributions and the associated transition weights. All of the calculations were carried out using Gaussian 09 package on a Power Leader cluster. Furthermore, the Multiwfn software was used to calculate the wave function of electron−hole pair from the transition density matrix (TDM) by TD-DFT and was plotted in a two-dimensional (2D) color-filled map for easily distinguishing the dimer ground- and excited-state character.

SI-3 Supplementary Figures and Tables

Table S1. Lifetimes of DMAC-NZC and DMAC-NZP in different solvents and in different conditions.

Materials/ Lifetimes (ns)	Hexane	n-butyl ether	Ethyl acetate	Tetrahydrofuran	5wt% PMMA film	crystal
DMAC-NZC	6.3	-	1.4	1.2	9.9	7.7
DMAC-NZP	11.6	12.5	2.0	-	12.5	2.6

Table S2. k_r and k_{nr} of DMAC-NZC and DMAC-NZP in different conditions. k_r = PLQY/Lifetimes, k_{nr} = (1-PLQY)/Lifetimes.

	DMAC-NZC			DMAC-NZP		
	solid	PMMA film	crystal	solid	PMMA film	crystal
PLQY(%)	4.3	71.2	3.2	35	74.9	5.7
Lifetimes(ns)	13.4	9.9	7.7	22.2	12.5	2.6
$k_r(10^8\ s^{-1})$	0.032	0.72	0.042	0.16	0.6	0.22
$k_{nr}(10^8\ s^{-1})$	0.71	0.29	1.3	0.29	0.2	3.6

Table S3. PLQY of DMAC-NZC and DMAC-NZP in powder, crystal 5% PMMA film, evaporated film and doped-film.

Materials/PLQY (%)	Powder	Crystal	5% doped in PMMA	Film	Doped-film
NZC	4.3	3.2	71.2	4.2	47.3
NZP	35	5.7	74.9	9.2	28.4

Data analysis

The fluorescence spectrum of luminogens are tested with the Edinburgh's FLs980 (in solution, in powder, in crystal, in 5% PMMA film). Generally, speaking, the luminogens which do not have dual-fluorescent phenomenon should not emit two peaks in the fluorescence spectra. However, most of the tested PL spectra show two emission peaks. To address this problem, we first measured the lifetimes of luminogen at the two emission peaks and we find the lifetimes at two peaks are basically same. In Figure S1(a) and Figure S1(b), the lifetimes of DMAC-NZP in hexane are 11.6 ns and 11.8 ns at 595 nm and 690 nm, respectively, so that we can consider they are the same, in other words, the two emission peaks are from the same excited state. Next, the "emission peak" at about 690 nm does not show any red shift with the increase of solution polarities (Figure 1b) while the real emission peaks demonstrate obvious red-shifts. Comparing to the measurements of the other red-emissive materials, we find that the peak position at 690 nm is caused by the **grating defect** of the instrument when the luminance of luminogens is not strong.

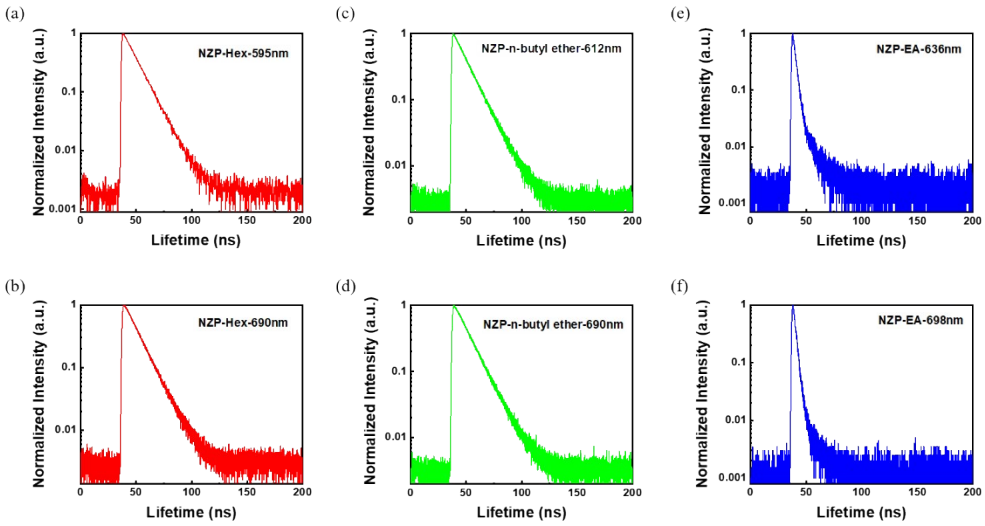

Figure S1. (a) Lifetime of DMAC-NZP in hexane at 595nm(11.6ns). (b) Lifetime of DMAC-NZP in hexane at 690nm(11.8ns). (c) Lifetime of DMAC-NZP in n-butyl ether at 612nm(12.5ns). (d) Lifetime of DMAC-NZP in n-butyl ether at 690nm(12.7ns). (e) Lifetime of DMAC-NZP in ethyl acetate at 639nm(2.0ns). (f) Lifetime of NZP in ethyl acetate at 698nm(2.1ns).

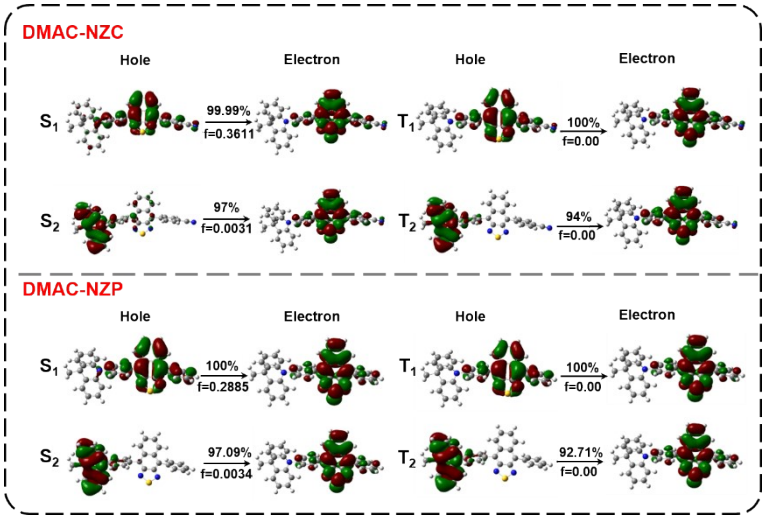

Figure S2. The natural transition orbitals of DMAC-NZC and DMAC-NZP.

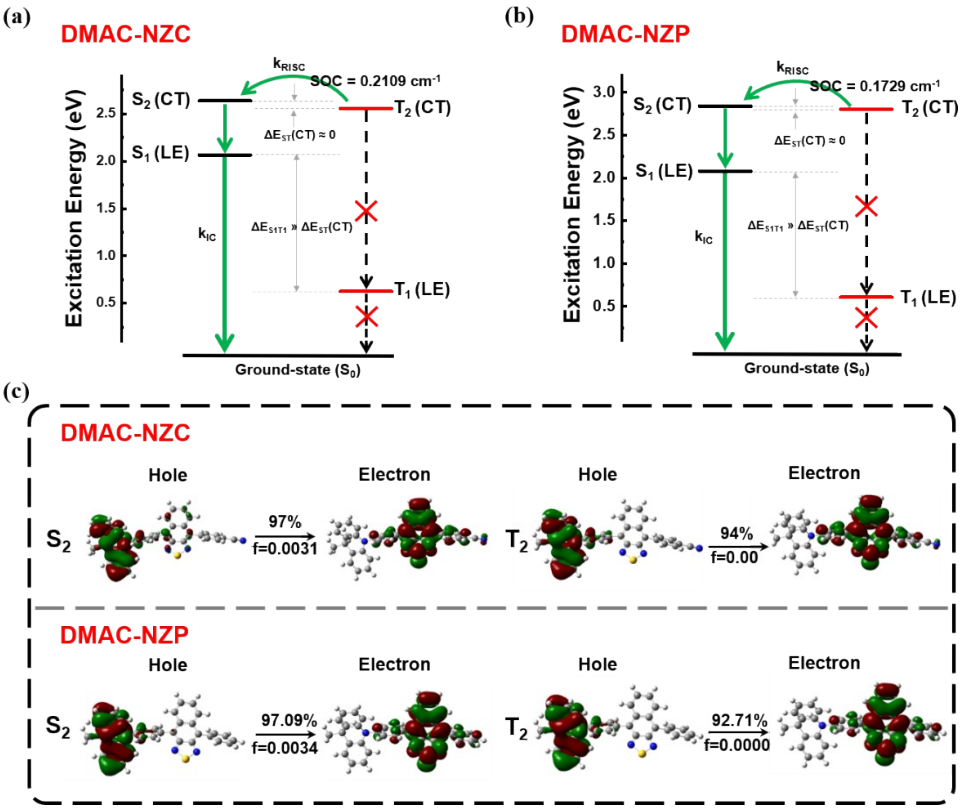

Figure S3. Molecular simulation on the excited states of DMAC-NZC and DMAC-NZP. (a) The excitation energy level of DMAC-NZC. (b) The excitation energy level of DMAC-NZP. k_{IC}: internal conversion rate; k_{RISC}: reverse intersystem crossing rate; LE: local excited state; CT: charge-transfer state; ΔE_{ST}: singlet–triplet energy splitting. (c) The NTO of the S_2 and T excited state of DMAC-NZC and the NTO of the S_2 and T_2 excited state of DMAC-NZP. The DFT and TDDFT calculations are carried out with a Gaussian 09 D. 01 package using the hybrid function m062x under 6-31g (d, p) level.

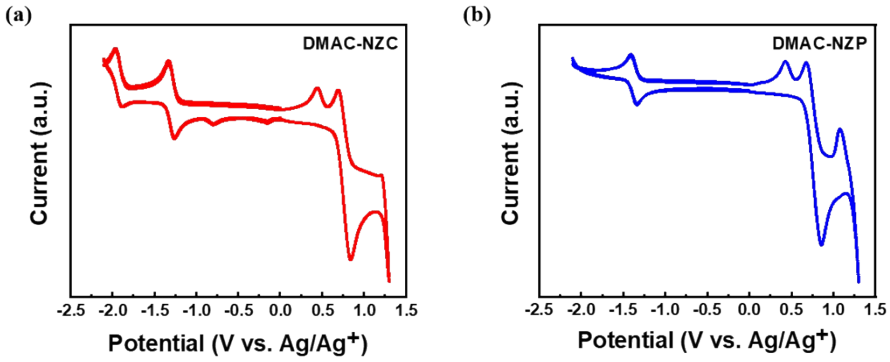

Figure S4. (a) Cyclic voltammograms of DMAC-NZC (HOMO: -5.23eV LUMO: -3.47eV), (b) Cyclic voltammograms of DMAC-NZP (HOMO: -5.20eV LUMO: -3.39eV) (measured in CH2Cl2 and DMF solution containing 0.1 M tetra-n-butylammonium hexafluorophosphate. Scan rate: 100 mV s^{-1}).

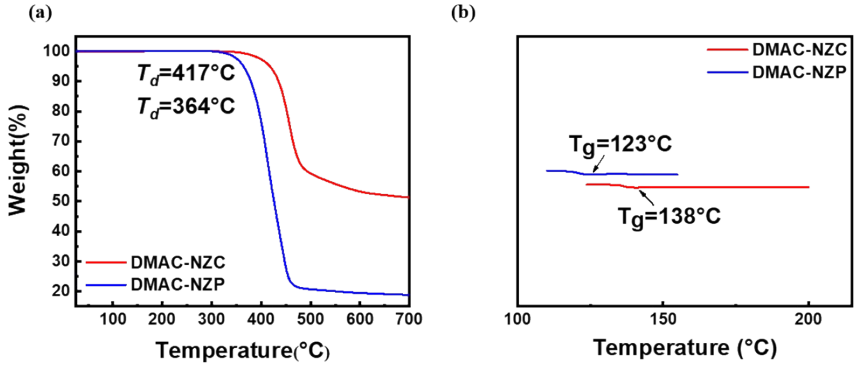

Figure S5. (a) Thermogravimetric analysis (TGA) of DMAC-NZC and DMAC-NZP (T_d: 5% weight loss temperature), (b) Differential scanning calorimetry (DSC) of DMAC-NZC and DMAC-NZP (T_g: glass transition temperatures).

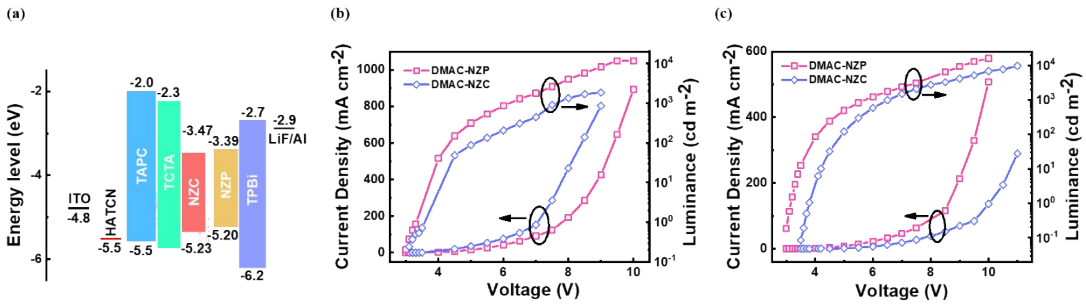

Figure S6. (a) Energy level of OLED structures, (b) Current density-voltage-lumiance(J-V-L) spectrogram of non-doped OLEDs, (c) Current density-voltage-

lumiance(J-V-L) spectrogram of doped OLEDs. In these structures, TAPC and TPBi are used as hole-transport layers and electron-transport layers, respectively, meanwhile, TPBi is also used as hole-blocking and exciton-blocking layers. HATCN is used as anode buffer layers for hole injection, while LiF is used as cathode buffer layers for electron injection.

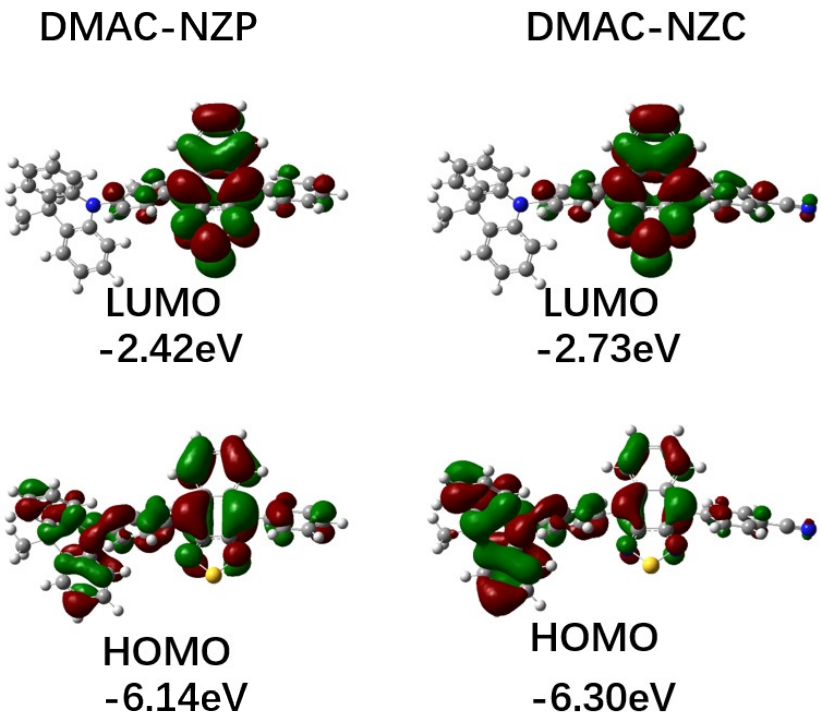

Figure S7. The frontier molecular orbital distributions of DMAC-NZC and DMAC-NZP.

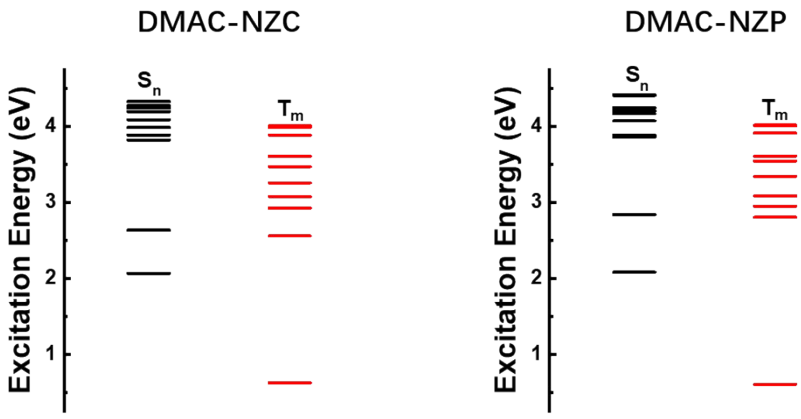

Figure S8. The excitation energy of DMAC-NZC and DMAC-NZP.

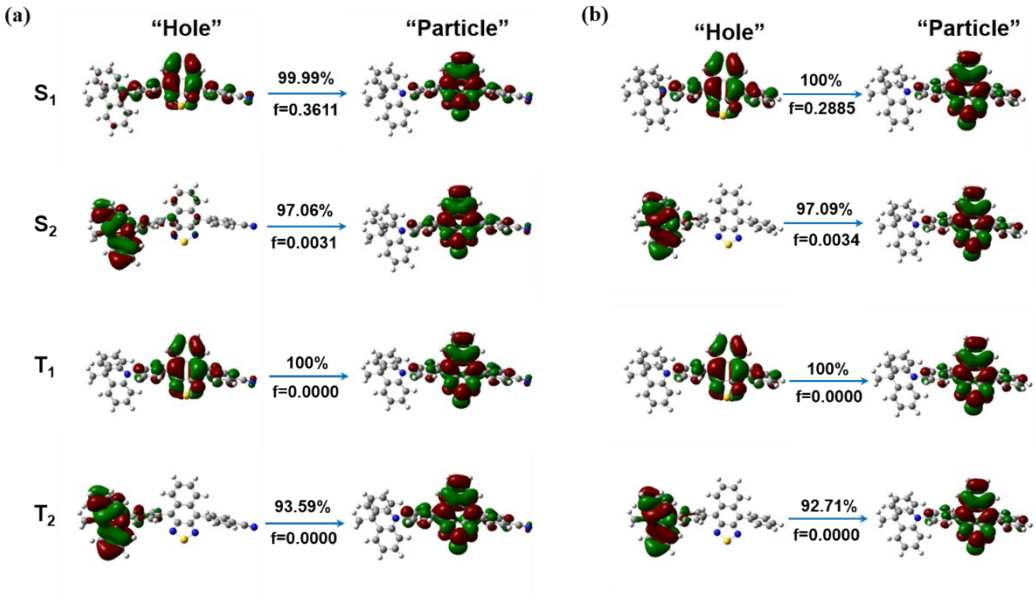

Figure S9. The natural transition orbits of DMAC-NZC and DMAC-NZP.

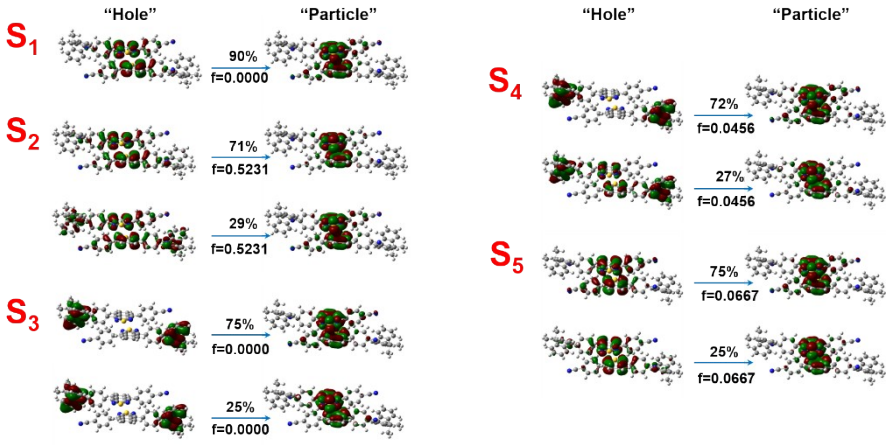

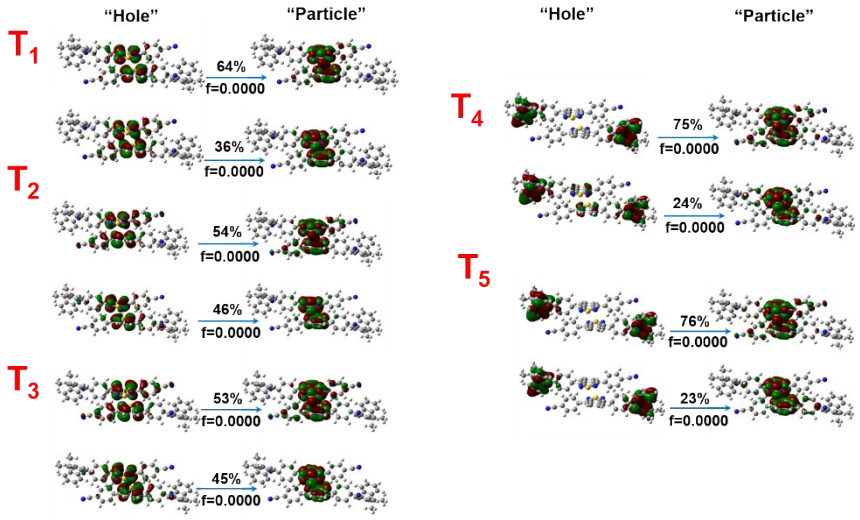

Figure S10. The natural transition orbits of DMAC-NZC dimer.

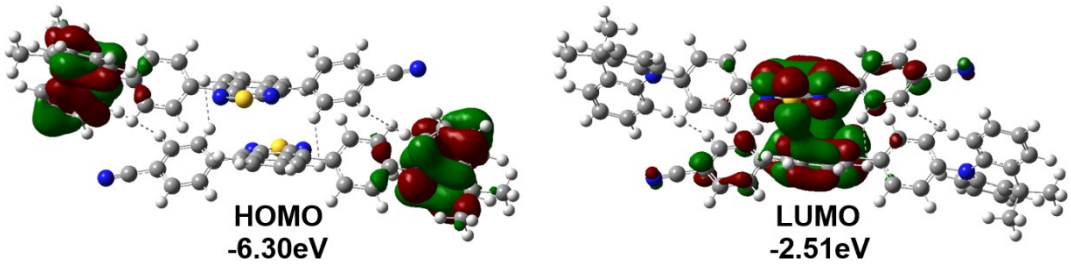

Figure S11. The frontier molecular orbital distributions DMAC-NZC dimer.

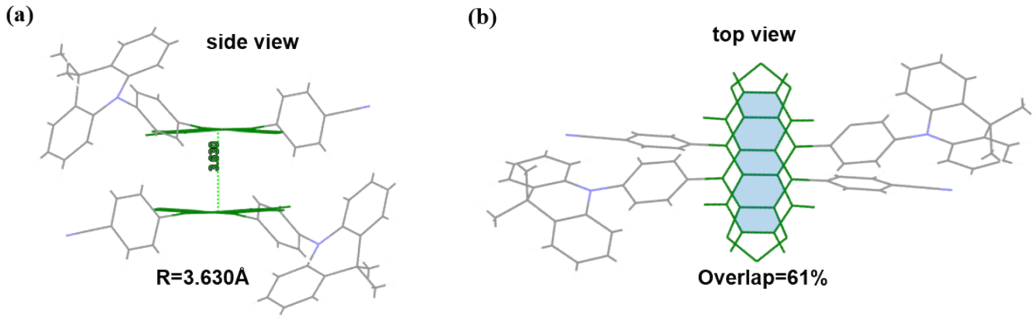

Figure S12. (a) The side view of DMAC-NZC dimer, (b) The top view of DMAC-NZP dimer.

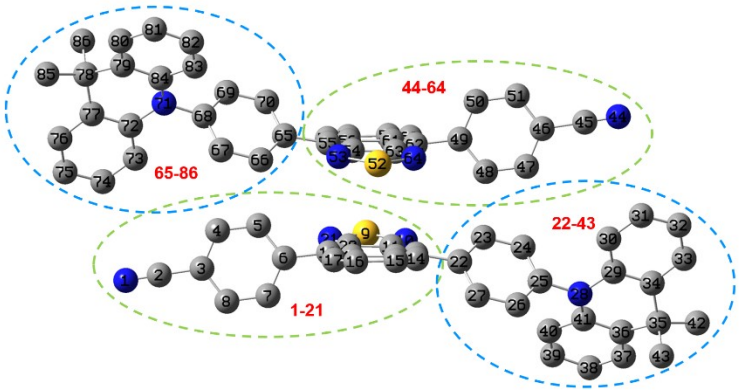

Figure S13. The labels of atoms in DMAC-NZC dimer.

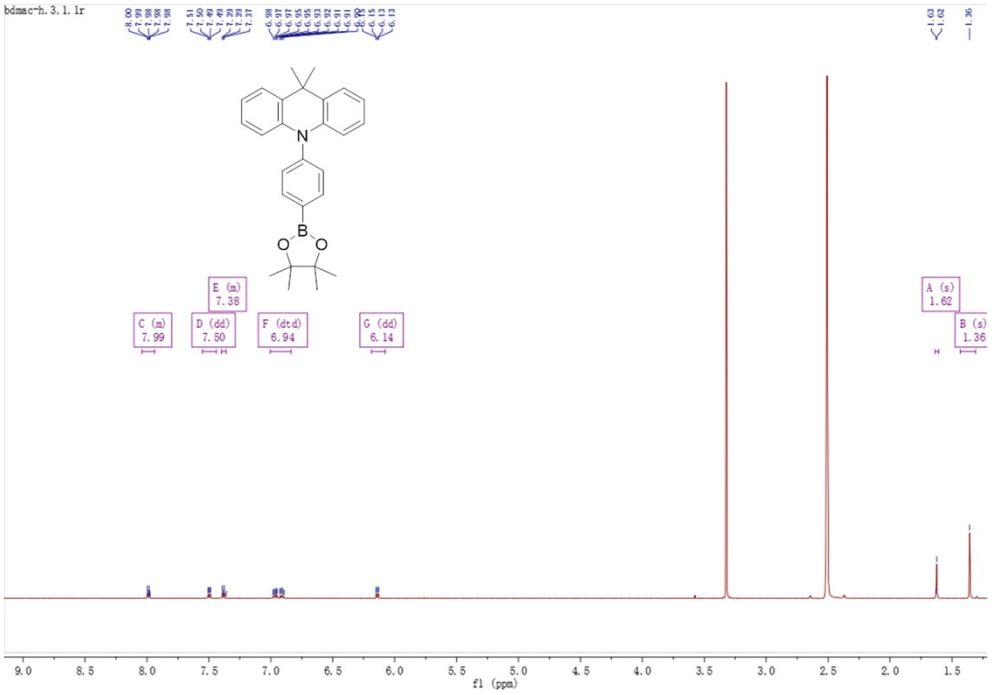

Figure S14. ^{1}H spectrums of B-DMAC in DMSO.

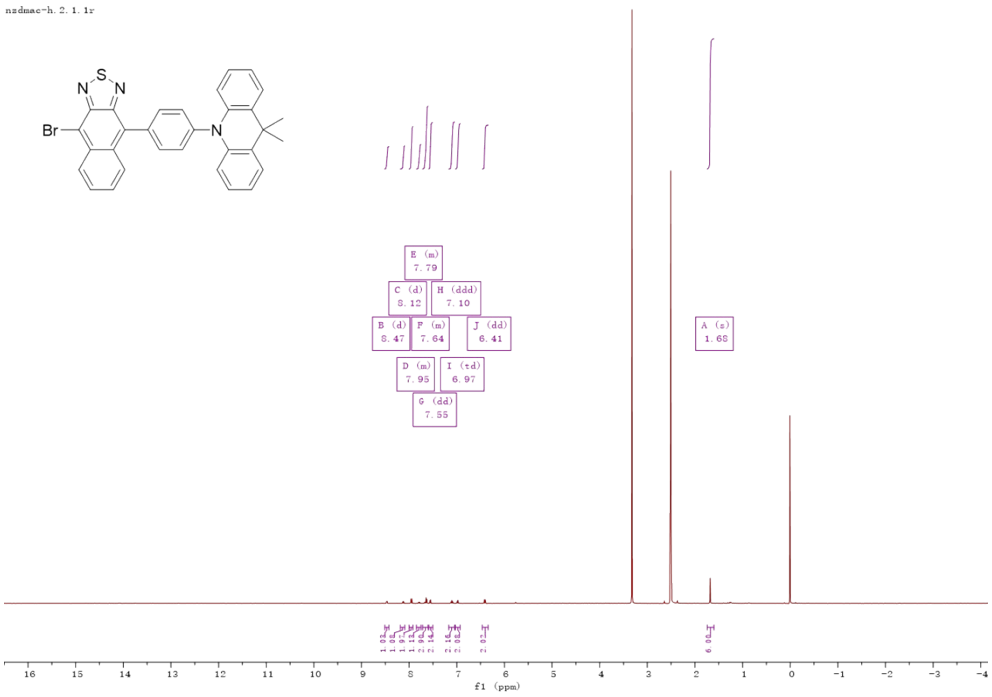

Figure S15. ^{1}H spectrums of NZ-DMAC in DMSO.

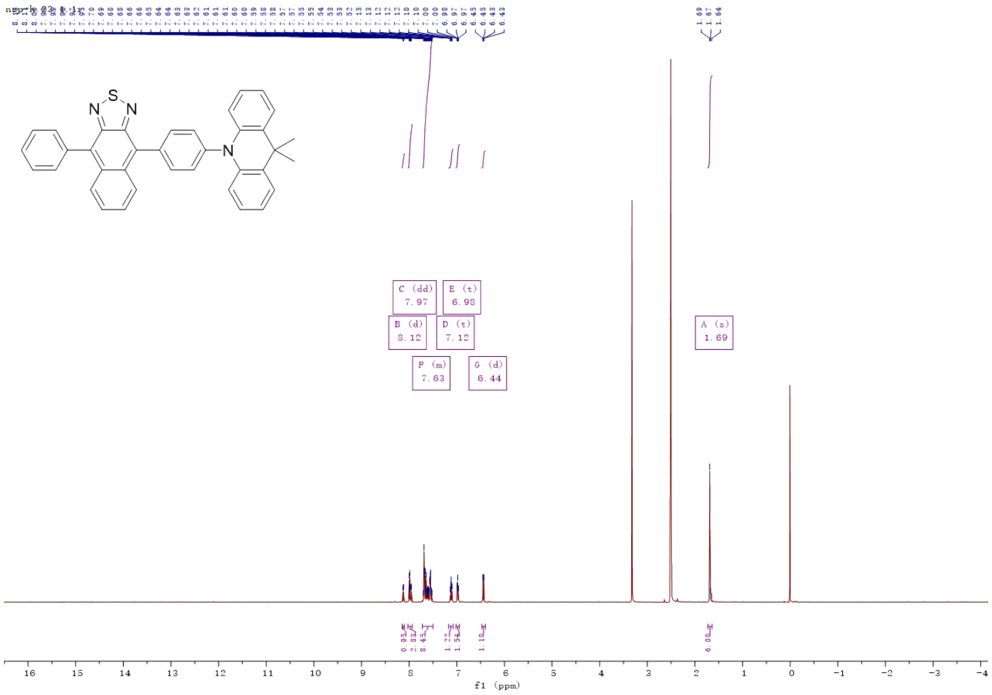

Figure S16. ^{1}H spectrums of DMAC-NZP in DMSO.

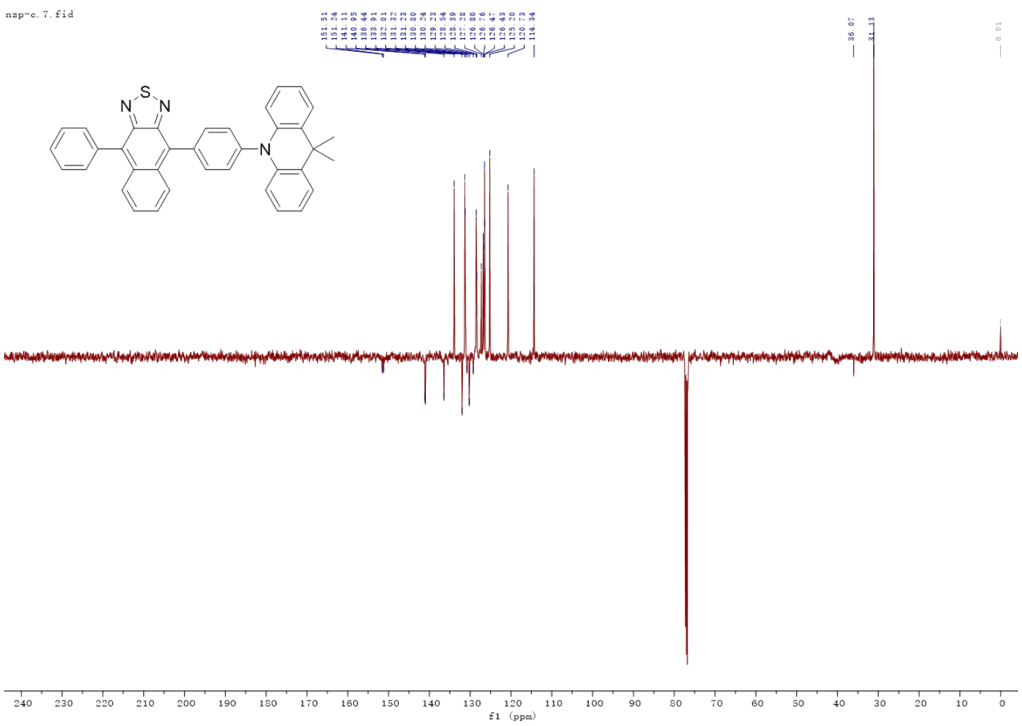

Figure S17. ^{13}C spectrums of DMAC-NZP in $CDCl_3$.

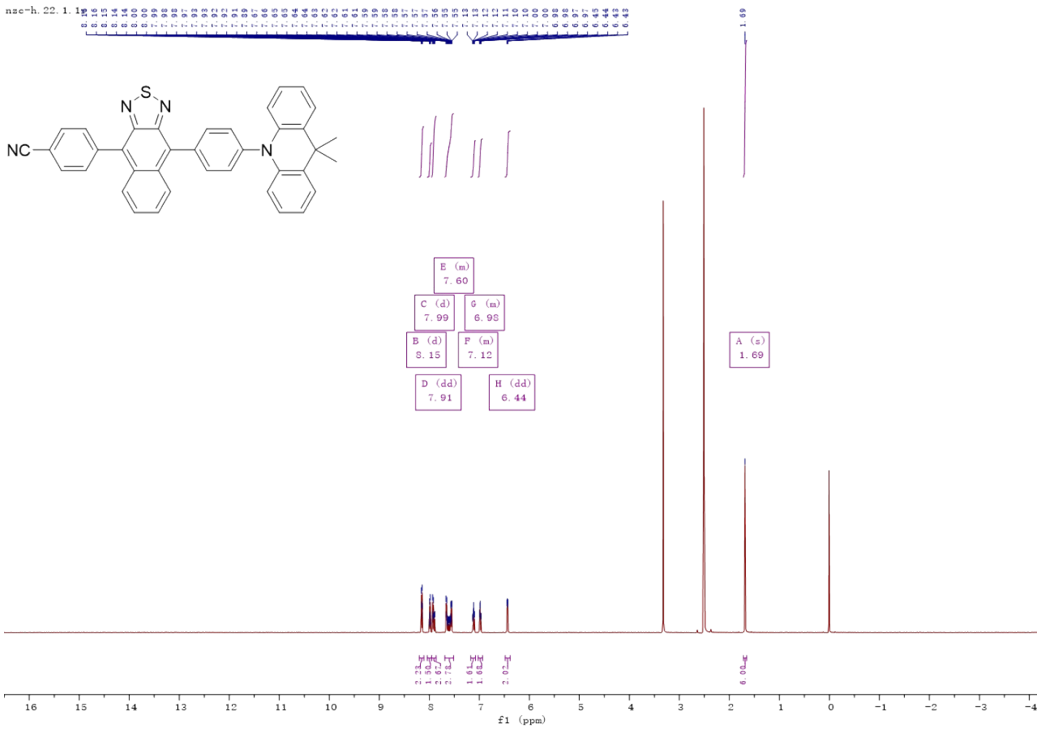

Figure S18. ^{1}H spectrums of DMAC-NZC in DMSO.

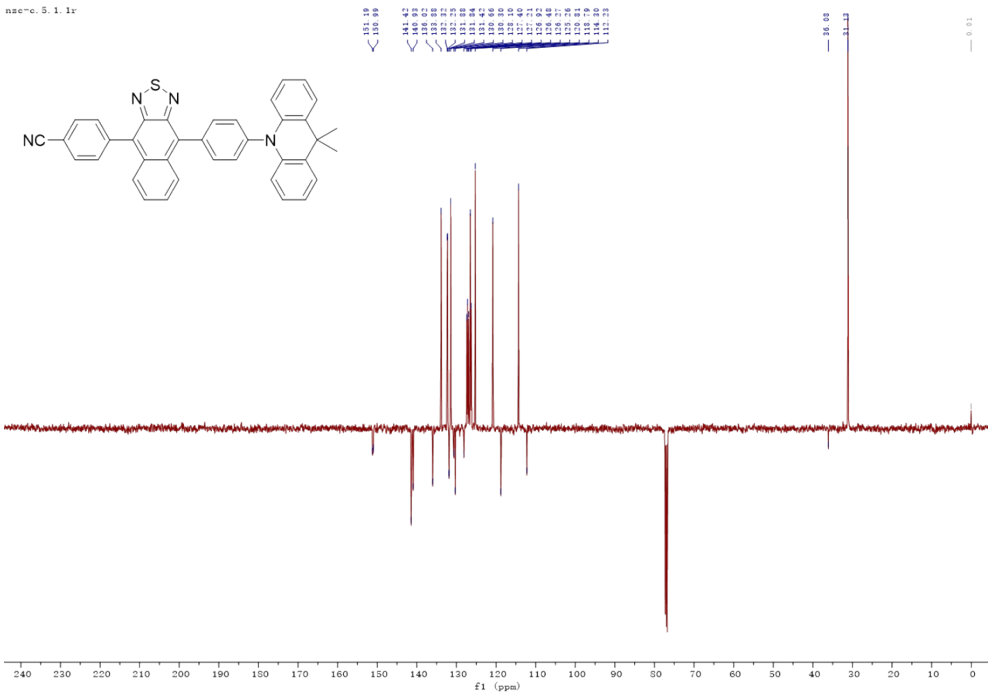

Figure S19. ^{13}C spectrums of DMAC-NZC in $CDCl_3$.